PROGRESS AND CHALLENGES FOR EMERGING INTEGRATED ENERGY MODULES

Titanium Dioxide Thin Films with Controlled Stoichiometry for Photoelectrochemical Systems

M. RADECKA,[1,4] A. BRUDNIK,[2] K. KULINOWSKI,[3] A. KOT,[1]
J. LESZCZYŃSKI,[1] J. KANAK,[2] and K. ZAKRZEWSKA[2]

1.—Faculty of Materials Science and Ceramics, AGH University of Science and Technology, Al. A. Mickiewicza 30, 30-059 Kraków, Poland. 2.—Faculty of Computer Science, Electronics and Telecommunications, AGH University of Science and Technology, Al. A. Mickiewicza 30, 30-059 Kraków, Poland. 3.—Faculty of Physics and Applied Computer Science, AGH University of Science and Technology, Al. A. Mickiewicza 30, 30-059 Kraków, Poland. 4.—e-mail: radecka@agh.edu.pl

The electrical resistivity of thin film metal oxide photoanodes in the photoelectrochemical cells, PEC, for hydrogen generation, the importance of which should not be neglected in the design and construction of water-splitting devices, is found to be affected by the departure from stoichiometric composition and film thickness. Here, we propose to use TiO_2/ITO photoanodes for photoelectrochemical cells. The TiO_{2-x} thin films with x indicating a departure from the stoichiometric composition have been prepared by dc magnetron sputtering with the deposition rate controlled by the optical emission spectroscopy, OES. Photoanode properties were determined by scanning electron microscopy, SEM, atomic force mocroscopy, AFM, Raman spectroscopy, transmittance and reflectance measurements over uv/vis/nir wavelength ranges, impedance spectroscopy, Mott–Schottky plots, and photocurrent versus voltage dependence in the dark and under white light illumination. The contributions of the charge carrier concentration and mobility to the enhanced photocurrent of the PEC have been determined and correlated to the varying film stoichiometry and thickness, respectively.

Key words: TiO_2, thin films, electrical resistivity, ITO

INTRODUCTION

Photoelectrochemical systems designed for hydrogen generation have been developed since the first realization in 1972 that efficient and reproducible photodecomposition of water could be carried out with the use of an auxiliary semiconducting photoanode such as TiO_2.[1] Since that time, enormous efforts and money have been dedicated to make this particular application of TiO_2 successful.[2–13] As a result of all these attempts, integrated solar-driven water-splitting devices have been developed and tested for hydrogen production on a laboratory scale.[14–19] Although, these experimental devices have entered the stage of commercialization, their mass fabrication has not been reached. The reason for that should be sought for in the properties of available photoanode materials and can be related to inefficient solar energy-to-hydrogen conversion processes.

An integrated solar-driven water-splitting device is generally comprised of light absorbers, electrocatalysts, membrane separators, and an electrolyte solution in a given system geometry.[15] Metal oxide photoanode that acts as a photon hv absorber and catalyst of reaction:

$$2hv + H_2O \rightarrow \tfrac{1}{2}O_2(gas) + H_2(gas) \qquad (1)$$
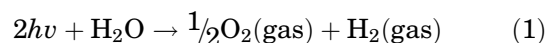
is one of the most important elements of the device. In order to generate oxygen and hydrogen by this process (Eq. 1), a thermodynamic potential of

1.23 eV is required.[1] As water is transparent to light over this wavelength range, the photons of at least 1.23 eV ($\lambda < 1000$ nm) should be absorbed by a semiconductor photoanode to generate electrons and holes in the respective conduction CB and valence VB bands:

$$hv \rightarrow e' + h^{\cdot}. \tag{2}$$

Therefore, the band gap energy of a semiconductor should be higher than 1.23 eV or even in between 1.8 eV and 2.4 eV taking into account all possible losses.[4,6,20] In order to run effectively the process of water splitting, the band edges of the semiconductor photoanode should fulfill the following condition: $E^{o}_{H+/H2} < E_{CB}$ and $E^{o}_{O2/H2O} > E_{VB}$. In spite of the fact that TiO_2 meets both these conditions, its main drawback is too wide a band gap which results in poor utilization of the solar spectrum and low solar energy-to-hydrogen conversion efficiency.[1,3,6]

Although at least four generations of photoanodes based on titania have been proposed,[4,5,21–23] there is still a limited success of this specific photoanode material. The first generation was based on undoped anatase/rutile and non-stoichiometric titanium dioxide. The next three generations of photoanode materials involved doping of either cationic (second generation), anionic (third generation) or both (fourth generation) sublattices.

However, there is one aspect, usually neglected, that should have a significant influence on the behaviour of the integrated solar-driven water-splitting device, which is an electrical resistance of the TiO_2 photoanode deposited on the substrate. In the case of transparent and conductive oxide substrates TCO, it is the resistance of the system: TiO_2 layer + TCO substrate that should be taken into account.

Electrical properties of TiO_2 thin films have been discussed in many papers.[24–35] It has been noted that the electrical resistivity is related to the sample non-stoichiometry.[34] Oxygen vacancies in the case of non-stoichiometric thin films of TiO_{2-x} are responsible for an increased charge carrier concentration.

However, as recently discussed,[35] much more attention should be paid to the charge carrier mobility. Widely-expanded opinion about very low electron mobility (< 1 cm^2 V^{-1} s^{-1} at room temperature) due to an extremely large effective mass within the range 30–100 m_e[24] has been recently verified. Dorow–Gerspach and Wuttig in their last paper[33] reported much higher electron mobility of 15 cm^2 V^{-1} s^{-1} for stoichiometric thin films of crystalline anatase TiO_2 obtained by reactive magnetron sputtering. Significant drop in the electron mobility to 0.06 cm^2 V^{-1} s^{-1} upon decreasing

relative oxygen level O_{2PP} below 55% has been attributed to the crystallographic disorder related to the amorphous phase formation.

We believe, that well-crystallized TiO_2 providing good electron mobility should play the most important role in the photoelectrochemical applications.

The motivation for the present study was to develop a clear description of the role the electrical resistivity of the TiO_2/TCO photoanode plays in photoelectrochemical water-splitting. Here, commercially available ITO substrates have been used as supports for thin films of TiO_{2-x} with controlled departure from stoichiometry. Thin films of TiO_{2-x} have been obtained by dc reactive sputtering from the Ti target in the Ar + O_2 atmosphere. The plasma emission controlled system provided reproducibility of the deposition conditions as far as the departure from stoichiometry was concerned. Variation of the film parameters such as their thickness and stoichiometry has been correlated with the morphology, crystallographic structure, optical and electrical properties with a special emphasis on the photoelectrochemical responses to illumination.

EXPERIMENTAL

Thin Film Deposition

Titanium oxide thin films were deposited onto specified substrates (amorphous silica a-SiO_2, indium tin oxide ITO, glass and Si) using a home built DC magnetron system.[36] The pure (5 N) titanium disc of 90 mm in diameter has been used as a sputtering target. The magnetron discharge was driven by dc-pulse power supply, working as a current source.[37] The distance between the target and substrate holder was kept at 50 mm. The substrates were heated before and during the film growth at the temperature of 250°C. High purity argon (6 N) and oxygen (5 N) were used as the sputtering and reactive gases, respectively. Gas flows were controlled by mass flow controllers. The base pressure of the system better than 5×10^{-6} mbar was attained with the turbomolecular pump. Sputtering was performed at a total pressure of 1×10^{-2} mbar. Magnetron current was stabilized at 2A with the sputtering power varying between 0.9 kW and 1.0 kW.

Optical emission spectroscopy (OES)[38] was used for controlling the deposition rate in order to stabilize the operating mode of sputtering. The optical emission of Ti ($\lambda = 500$ nm) line intensity in the pure argon discharge (no flow of oxygen) was used as a reference for monitoring the OES system.

The oxygen flow was controlled by setting the current titanium emission line intensity at a predefined value. The ratio I/I_0 correlates with the sputtering rate[2,39,40] and corresponds to the deviation from stoichiometry x in TiO_{2-x}. Higher

I/I_0 indicates more oxygen deficient compositions as shown in Ref. 41.

Techniques Employed for Determination of the Photoanode Properties

The thickness of the deposited thin films was measured by a Talystep (Rank Taylor Hobson) stylus profilometer. The scanning electron microscope SEM morphological studies were carried out using Nova NanoSem 200 instrument equipped with an energy dispersive x-ray spectroscope.

The surface morphology was studied with an atomic force microscope (AFM) in semi-contact mode using a NTEGRA Aura—NT-MDT system. Root mean square (RMS) was calculated.

Raman spectra were collected using Witec Alpha 300 M+ spectrometer equipped with $100\times$ objective and 1800 grating. Incident light excitation at the wavelength of 488 nm was provided by a laser. Raman spectra were recorded upon two accumulations within the range of wavenumbers extending from 1 cm^{-1} to 4000 cm^{-1}.

Transmittance and reflectance spectra of ITO, $TiO_2'ITO$ and $TiO_2/a\text{-}SiO_2$ were measured by a Perkin Elmer Lambda 19 spectrophotometer within the wavelength range of 220–2500 nm.

Impedance spectroscopy data were acquired by means of the dielectric interface Solartron 1296 and frequency response analyser Solartron 1260. Two different configurations were tested. The impedance measurements to determine the electrical resistance were performed over the frequency range of $1–10^6$ Hz at room temperature. Two gold point electrodes separated by a distance of 10 mm were applied. Moreover, the capacitance of the electrode/electrolyte interface as a function of the voltage in the photoelectrochemical cell PEC was studied using the same equipment (Solartron 1260 + Solartron 1296). In this case, the measurements were performed in the dark at a constant frequency of 10 kHz. Analysis of the impedance spectra was carried out with the help of the ZPLOT software provided by Solartron and dedicated for this purpose.

Functional Measurements: Photocurrent Versus Applied Voltage

Photoelectrochemical experiments in the dark and under illumination were performed in a custom-made photoelectrochemical cell PEC. A three-electrode cell was employed, with the working anode based on TiO_2/ITO thin films, a saturated calomel electrode (SCE) as a reference electrode, and a Pt foil covered with a Pt black acting as a cathode. A Na_2SO_4 solution (0.8 M, pH = 6.25) was used as the electrolyte. The PEC was illuminated with a white light provided by a 450 W Xe lamp. An ANKO potentiostat was used for the current–voltage measurements.

RESULTS AND DISCUSSION

Optical and electrical characterizations of ITO substrates have been performed, and the results of the analysis are shown in Fig. 1.

The ITO substrate exhibits high transparency within the wavelength range of 400–1000 nm and high reflectivity in the infrared IR region (Fig. 1a). From the region of the fundamental absorption edge, the band gap of ITO has been determined to be of about 4.11 eV in accordance with the literature data.[42–44] High concentration of electrons results in the plasma reflectance edge quite clearly seen in the near infrared as an abrupt increase in reflectance coefficient R accompanied by a decrease in the transmittance T. Interaction of light with the electron cloud can be understood on the basis of the classical Drude's model.[45]

The plasma resonance wavelength λ_p was obtained as a cutoff wavelength, at which $T(\lambda_p) = R(\lambda_p)$. Under these conditions, the dielectric-like visible transmittance is the same as the metallic-like IR reflectance.

The plasma resonance frequency ω_p is given by

$$\omega_p^2 = \frac{Ne^2}{\varepsilon_0 \varepsilon_\infty m^*}, \qquad (3)$$

where ε_∞ and ε_0 represent the dielectric constants of the ITO and a free space, respectively, m^* is the effective mass of the charge carriers, and N is the carrier concentration.

The relationship between the plasma resonance wavelength λ_p and plasma resonance frequency ω_p is given as:

$$\lambda_p = \frac{1240}{\hbar \omega_p} = \frac{1240}{h\nu_p}, \qquad (4)$$

where $\omega_p = \nu_p \cdot 2\pi$ and the photon energy $h\nu_p$ is expressed in eV.

For ITO it was assumed that $\varepsilon_\infty = 4$, $m^* = 0.3\, m_0$, while plasma resonance wavelength was calculated as $\lambda_p = 1380$ nm which corresponds to $h\nu_p = 0.90$ eV.

The charge carrier concentration computed from (3) has been found to be $N = 7.02 \times 10^{20}\ cm^{-3}$, which remains within the limits of the literature data.[43,44]

Further characterization of ITO was carried out by means of the electrical measurements of Mott–Schottky plots C^{-2} versus V_B, impedance spectroscopy $|Z|$ versus f or admittance Y'' (imaginary part) versus Y' (real part), current I—voltage V_B as well as photoelectrochemical measurements of current I versus voltage V_B in dark and under white light illumination. The results of these investigations are shown in Fig. 1b–e.

The electrical resistance of the ITO substrate has been determined from the Mott–Schottky plots to be of about 22.5 Ω independently of the applied voltage. The same conclusion could be drawn from the linearity of I–V characteristics indicating ohmic
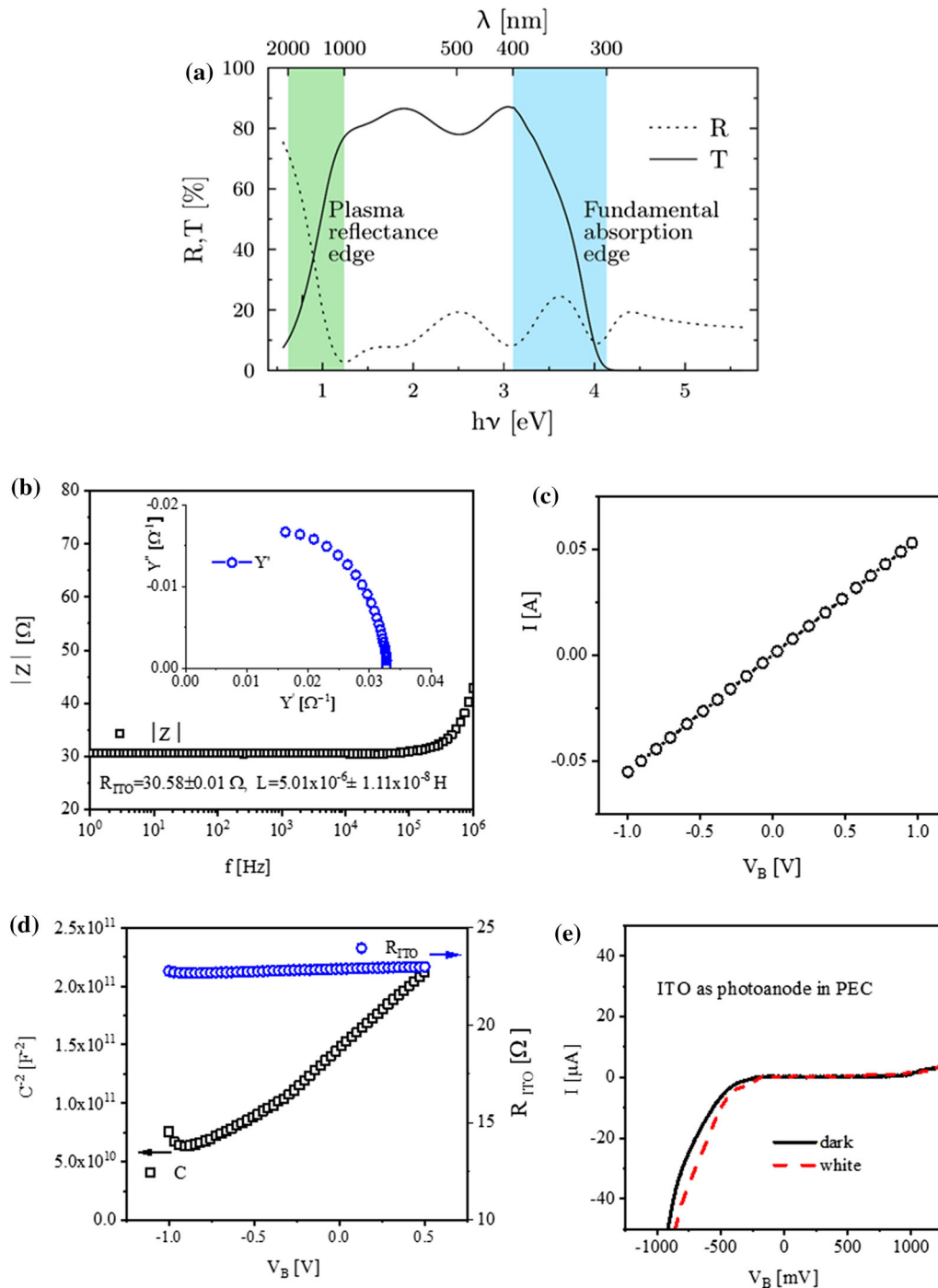
Fig. 1. Optical and electrical characterization of the ITO substrate; transmittance T and reflectance R spectra (a), impedance spectra: $|Z|$-absolute value of the impedance; f-frequency, Y'-real, Y''-imaginary parts of the admittance. The inset shows Nyquist plot (b) I–V_B characteristics (c), Mott–Schottky plot and resistance of ITO versus applied voltage V_B (d) and current versus voltage dependence for PEC with a photoanode based on ITO (e).

behaviour of the ITO electrode. A quite similar result has been obtained from the impedance spectra that could have been fitted with a simple equivalent circuit consisting of a resistor of about 30 Ω and an inductance of about 5 μH.

As far as the carrier concentration is concerned, its value derived from the Mott-Schottky plots is of

about 1.4×10^{21} cm^{-3} which is almost of the same order of magnitude as that determined from the plasma reflectance edge, Eq. 3.

From the I–V_B plots in dark and under illumination, performed in the three-electrode photoelectrochemical cell described in the experimental subsection "Functional Measurements: Photocurrent

Versus Applied Voltage", it can be concluded that the ITO substrate is suitable for the construction of the more complex electrodes especially for TiO_2/ITO photoanodes. In this case, both the anodic part of photocurrent and the dark current are close to zero, therefore, we make sure that the ITO substrate does not contribute to the processes of water splitting in the PEC device.

The Raman spectra of the TiO_2/ITO photoanodes (Fig. 2) allow us to study their structural properties from the point of view of polymorphic forms crystallizing under oxidizing (I/I_0= 0.16) and slightly under-oxidized (I/I_0= 0.20) conditions of the film growth. In all these cases, only the anatase form can be distinguished which manifests itself by the presence of five characteristic Raman peaks at 144 $E_{g(1)}$, 196 $E_{g(2)}$, 396 $B_{1g(1)}$, 516 $A_{1(g)}$, and 638 $E_{g(3)}$ cm^{-1}.[46] The tendency towards amorphisation is clearly seen in the case of slightly non-stoichiometric TiO_{2-x} obtained at I/I_0= 0.20 where only the 144 cm^{-1} Raman peak can be distinguished. Moreover, the influence of TiO_2 film thickness on the structure ordering is clearly seen. Higher thickness of stoichiometric films obtained at I/I_0= 0.16 results in better crystallization of anatase polymorphic form. Under these growth conditions we do not expect rutile to be present.[2]

Figure 3 presents SEM images of the top surface of ITO substrates and TiO_2/ITO photoanodes at different magnifications. Typical morphology of transparent conductive metal oxide is clearly demontrated in the case of ITO. The grains visible in scanning electron micrographs are small with a diameter of about 30 nm. Very thin films (d = 50 nm) of stoichiometric TiO_2 follow the pattern imposed by ITO. However, larger film thickness (d = 280 nm) allows one to observe the morphology characteristic for TiO_2. The TiO_2 forms a dense layer composed of nano-agglomerates.

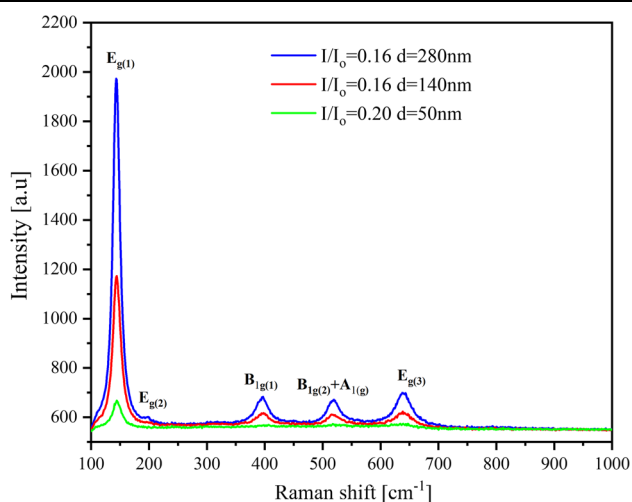AFM images (Fig. 4) of bare ITO substrate and TiO_2 thin films of different thickness deposited on ITO confirm the conclusions drawn from SEM (Fig. 3). The roughness of ITO substrate (RMS = 3.230 nm) is reduced to RMS = 2.347 nm when covered by a very thin film of TiO_2 (d = 50 nm). For thicker TiO_2 films (d = 280 nm) the surface roughness increases to RMS = 2.832 nm because of the pronounced influence of the columnar film growth.

Optical properties of TiO_2/ITO photoanodes have been studied by analyzing the transmittance $T(\lambda)$ and reflectance $R(\lambda)$ spectra over the wide wavelength range extending from the ultraviolet to near infrared region as shown in Fig. 5a. However, as the optical properties of the ITO substrate dominate the optical spectra of TiO_2/ITO, which manifest itself in the plasma reflectance edge and the interference fringes observed in both $T(\lambda)$ and $R(\lambda)$, it was necessary to deposit TiO_2 on featureless substrate such as an amorphous silica a-SiO_2 (Fig. 5b). For a very thin stoichiometric TiO_2 film one can observe the fundamental absorption edge extending from 300 nm to 400 nm which corresponds to the band gap of anatase of about 3.2–3.4 eV. The values of the band gap E_g for TiO_2 (Table I) thin films of variable thickness and stoichiometry differ from those reported for crystalline anatase, which is due to the nanocrystalline nature of the films obtained. Very thin, stoichiometric films of TiO_2 reach very high transmittance coefficients in the near infrared, $T(\lambda = 2200$ nm$) = 90\%$ while the reflectance coefficient is very low, $R(\lambda = 2200$ nm$) = 10\%$ which indicates no light absorption. Due to a very high refractive index of TiO_2, $n > 2.2$, the reflectance coefficient is quite elevated in the visible range of the light spectrum ($R = 40\%$ for 400 nm $< \lambda <$ 500 nm). Moreover, even at this small thickness d = 50 nm, the wavelength modulation in T and R attributed to the light interference, is clearly seen.

Impedance spectra for TiO_2/ITO photoanodes in Nyquist and Bode configurations are given in Fig. 6. The spectra demonstrate a typical semiconducting behavior, thus they have been fitted with an equivalent circuit consisting of the electrical resistor and capacitance elements in series. Small capacitance C of TiO_2 of the order of 10^{-11} F is characteristic for dielectric processes taking place in this material. The electrical resistance decreases systematically with the increasing film thickness. The electrical resistivity ρ as a function of the films thickness and stoichiometry, given in Table I, has been determined from the impedance spectra.

It should pointed out at this stage that it is impossible from these data to assess the contributions of charge carrier concentration N and mobility μ to the electrical resistivity. This could be done if the charge carrier concentration were derived from independent measurements of, for example, Mott–Schottky plots (Fig. 7a). From the slope of C^{-2} versus V_B dependence the concentration of the charge carriers can be calculated according to the formula:
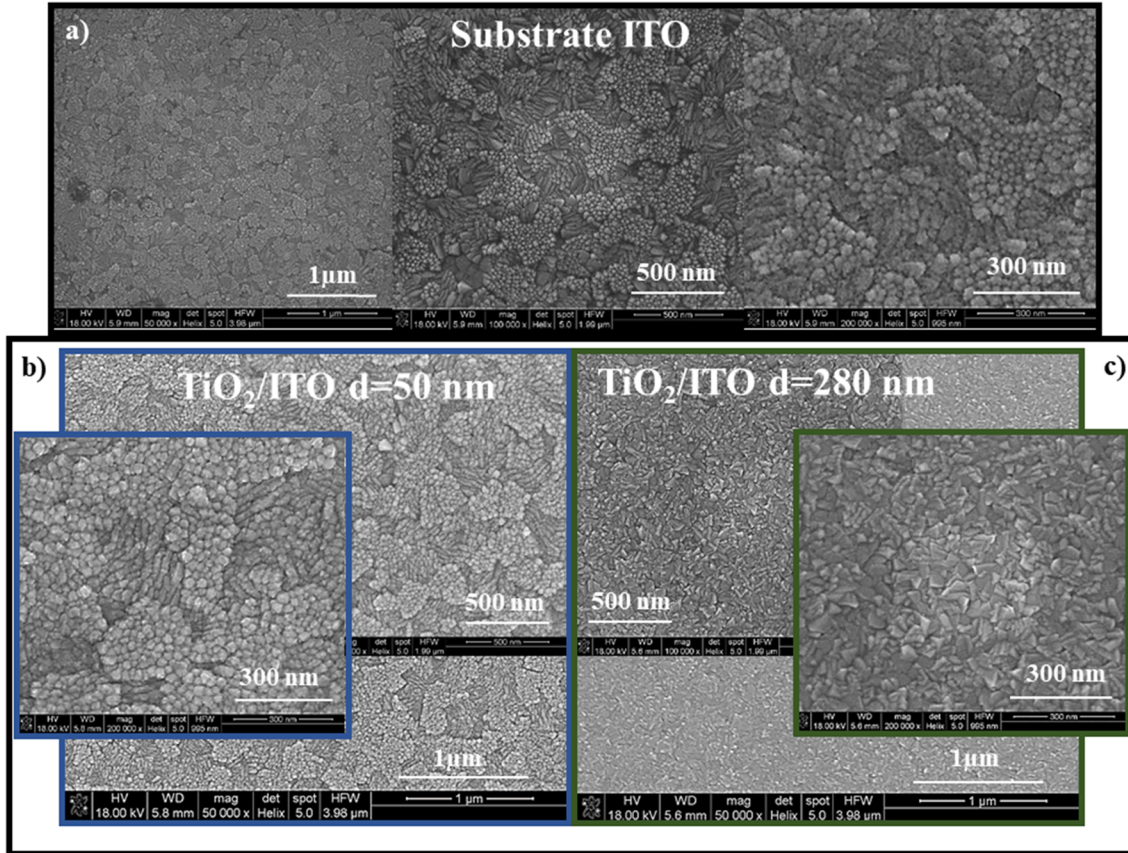

Fig. 2. Raman spectra for TiO_2/ITO photoanodes.

Fig. 3. SEM top surface images of ITO substrate (a) and TiO$_2$/ITO photoanodes: thin film thickness d = 50 nm (b) and d = 280 nm (c).

$$C_{SC}^{-2} = \left(\frac{2}{\varepsilon\varepsilon_0 eNS^2}\right)\left(V_B - V_{FB} - \frac{kT_A}{e}\right), \qquad (5)$$

where T_A is the absolute temperature, k is the Boltzmann constant, $S = 1$ cm^2 is an area of the electrode.

The positive slope of C^{-2} versus V_B for TiO$_2$/ITO photoanodes indicates the n-type conductivity of deposited TiO$_2$ thin films. The results of N calculations are included in Table I.

The current–voltage characteristics for TiO$_2$/ITO photoanodes shown in Fig. 7b prove that this electrode fulfills the requirements for a correct performance of the photoelectrochemical cell, PEC. The dark current is small, the cathodic current is negative while the anodic photocurrent is positive and much higher than the dark current in this configuration. The flat band V_{FB} potential determined as a photocurrent onset (see Fig. 7b) is negative for all photoanodes discussed in this work.

There are numerous experimental methods of the flat band potential estimation. They include: illuminated OCP (open circuit potential), Mott–Schottky analysis without illumination and the photocurrent onset. However, due to certain limitations of each technique, the values of V_{FB} resulting from these different methods can be in some disagreement. From the Mott-Schottky plot, the flatband potential V_{FB} can be obtained as the intercept of $(C)_{-2}$ with the V_B-axis.

The values of the flat band potential obtained from the Mott–Schottky plots are also included in Table I. Comparing them with the flat band potential determined from the photocurrent only, one can see that V_{FB} shifts towards more negative values. The photocurrent onset is the method based on the fact that upon photogeneration of the electron–hole pairs in the semiconductor, the bands become less bent. In the vicinity of flat band potential V_{FB} the recombination process may suppress the photocurrent. In fact, the measured capacitance does not necessarily correspond to the exact value of the space charge capacitance C_{sc} due to the contribution of other capacitances such as that of the Helmholtz layer, the Gouy layer, surface states, deep donor levels, and dielectric relaxation. Therefore, it would be advantageous to use an alternative method to check the value of V_{FB} derived from the capacitance potential studies.

The influence of stoichiometry and thickness of TiO$_2$ thin films on the V_{FB} can be seen in Table I. As a general rule, stoichiometric thin films, with the smallest crystallographic disorder, possessing the highest charge carrier mobility, demonstrate the
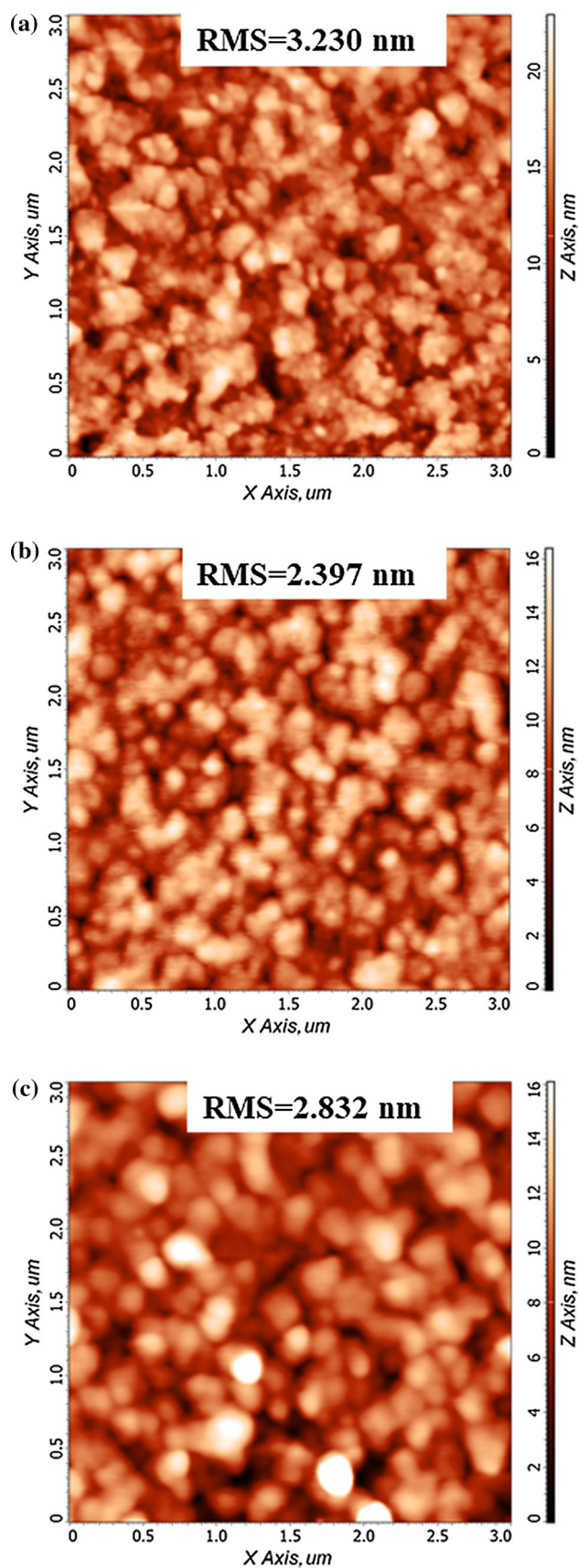
Fig. 4. AFM surface images of ITO substrate (a) and TiO$_2$/ITO photoanodes: film thickness d = 50 nm (b) and d = 280 nm (c).
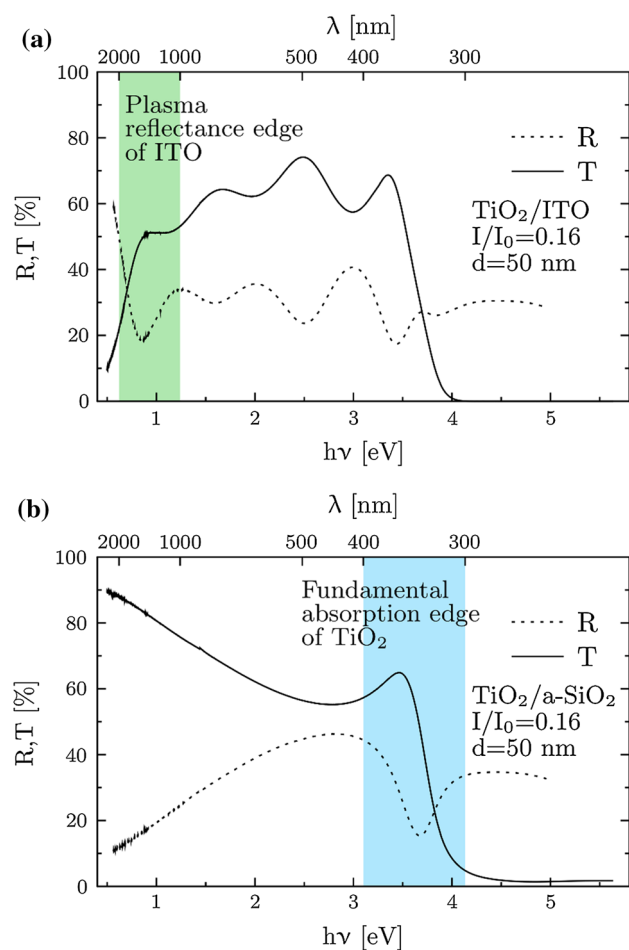

Fig. 5. Spectral dependence of optical transmittance and reflectance of TiO$_2$/ITO (a) and TiO$_2$/a-SiO$_2$ photoanode (b).

best photocurrent–voltage characteristics and the most negative flat band potential.

Figure 8 summarizes the results obtained in the course of this work. The photocurrent I_{ph} values at V_B= 0 V have been found to be correlated with the electrical resistivity ρ of TiO$_2$/ITO photoanode. As a general conclusion, one can state that the lower the value of the electrical resistivity, the higher the value of the photocurrent. However, the contribution of the charge carrier concentration and mobility to the photocurrent dependence on the electrical resistivity is different. In the case of stoichiometric thin films of TiO$_2$ deposited at I/I_0= 0.16 onto ITO substrates, the increasing film thickness is accompanied by the improved crystallographic ordering and the increased charge carrier mobility (Fig. 2, Table I). The photocurrent increase in this case can be explained by a substantial improvement of the charge carrier mobility. In the case of nonstoichiometric TiO$_{2-x}$ thin films of the same thickness, the charge carrier concentration increase is not sufficient to bring the photocurrent to the required level. The charge carrier mobility in the case of nonstoichiometric thin films of TiO$_2$ deposited at I/I_0= 0.20 onto ITO

Table I. Basic parameters of TiO_2 thin films on ITO substrate

I/I_0	d (nm)	ρ ($\Omega \cdot$cm)	$N \cdot 10^{18}$ (cm^{-3})	V_{FB} (V) from $I-V$	V_{FB} (V) from $M-S$	μ (cm^2 V^{-1} s^{-1})	E_g (eV)
TiO₂							
0.16	50	14,000	8.10	-0.52	-0.72	5.50×10^{-5}	3.54
	140	9618	0.73	-0.72	-0.81	8.85×10^{-4}	3.42
	280	3920	0.69	-0.62	-0.79	2.29×10^{-3}	3.41
0.20	50	3337	12.48	-0.51	-0.74	1.50×10^{-4}	3.63
ITO							
	250	5.75×10^{-3}	702			1.54	4.11
			1397[a]			0.78	

[a]From Mott–Schottky plots, d—film thickness, ρ—electrical resistivity, N—carriers concentration, V_{FB}—flat band potential, μ—mobility, E_g—band gap.
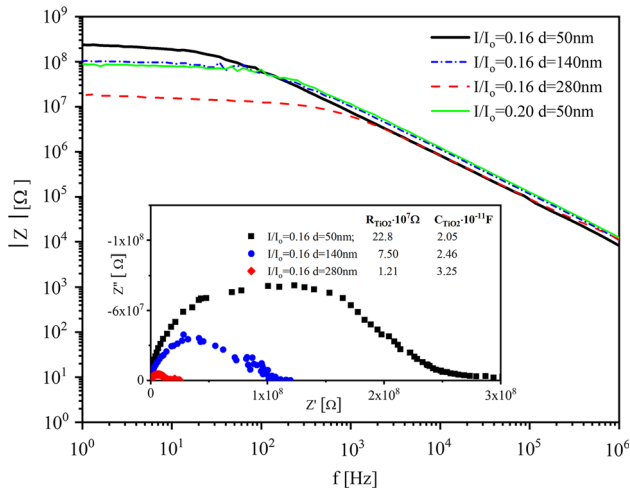

Fig. 6. Impedance spectra of TiO₂/ITO photoanodes; |Z|—absolute value of the impedance; f—frequency, Z′—real, Z″—imaginary parts of the impedance, d—thin film thickness. The inset shows a Nyquist plot.

Fig. 7. Characterization of TiO₂/ITO photoanodes: Mott–Schottky plot (a) and current versus voltage dependence (b).

substrates is lower than that for the stoichiometric ones sputtered at $I/I_0 = 0.16$ as shown in Table I, due to a certain structural disorder accompanied by an increased number of scattering centers.

CONCLUSIONS

This work was devoted to TiO₂/ITO photoanodes acting as elements of the integrated solar-driven water splitting devices for hydrogen generation. The importance of the electrical resistivity to the photo-electrochemical processes has been elucidated. It has been demonstrated that the ITO substrate is suitable as a support for thin film metal oxide electrodes, because it does not contribute to the photocurrent under white light illumination. Its transparency over the uv/vis/nir region of the light spectrum combined with the high electrical conductivity fulfills the requirements for the efficient photoanode substrate. As far as TiO$_{2-x}$ thin films
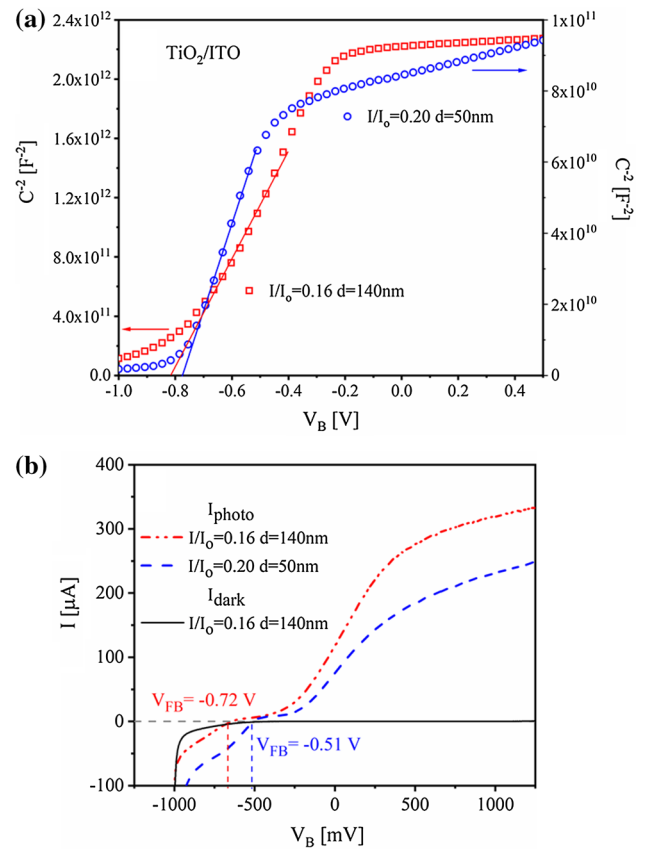
deposited by dc magnetron sputtering are concerned, it has been found that their thickness was correlated with the charge carrier mobility, μ while the increased departure from stoichiometry x resulted in the elevated charge carrier concentration, N. The photocurrent increase with the film thickness has been attributed to an increased
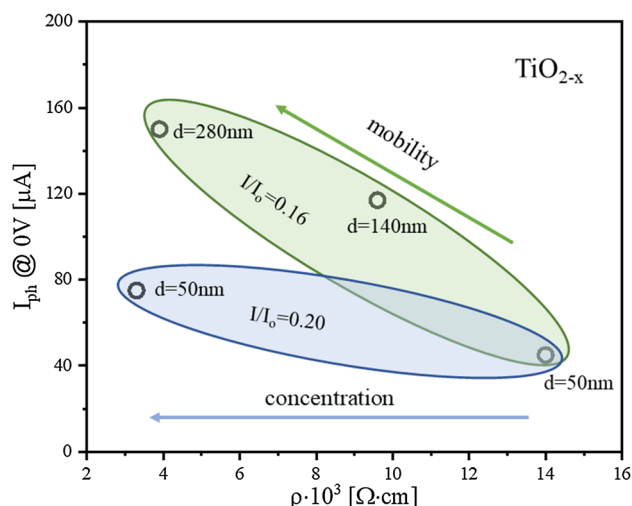
Fig. 8. Photocurrent I_{ph} *versus* electrical resistivity ρ of TiO_2/ITO photoanodes.

charge carriers' mobility and improved film ordering. On the other hand, the film non-stoichiometry leading to the elevated charge carrier concentration creates the crystallographic disorder that reduces partly the growth of the photocurrent.

ACKNOWLEDGMENTS

OPEN ACCESS

REFERENCES

1. A. Fujishima and K. Honda, *Nature* 238, 37 (1978).
2. A. Brudnik, A. Gorzkowska-Sobas, E. Pamula, M. Radecka, and K. Zakrzewska, *J. Power Sources* 173, 774 (2007).
3. M. Radecka, M. Rękas, A. Trenczek-Zając, and K. Zakrzewska, *J. Power Sources* 181, 46 (2008).
4. M. Radecka, A. Kusior, A. Trenczek-Zajac, and K. Zakrzewska, *Adv. Inorg. Chem.* 72, 145 (2018).
5. A. Kusior, A. Wnuk, A. Trenczek-Zając, K. Zakrzewska, and M. Radecka, *Int. J. Hydrogen Energy* 40, 4936–4944 (2015).
6. J. Li and N. Wu, *Catal. Sci. Technol.* 5, 1360 (2015).
7. Y. Ma, X. Wang, Y. Jia, X. Chen, H. Han, and C. Li, *Chem. Rev.* 114, 9987 (2014).
8. H. Ahmad, S.K. Kamarudin, L.J. Minggu, and M. Kassim, *Renew. Sustain. Energy Rev.* 43, 599 (2015).
9. J. Schneider, M. Matsuoka, M. Takeuchi, J. Zhang, Y. Horiuchi, M. Anpo, and D.W. Bahnemann, *Chem. Rev.* 114, 9919 (2014).
10. W. Fang, M. Xing, and J. Zhang, *J. Photochem. Photobiol., C* 32, 21 (2017).
11. R. Shwetharani, M. Sakar, C.A.N. Fernando, V. Binas, and R.G. Balakrishna, *Catal. Sci. Technol.* 9, 12 (2019).
12. S. Shen, J. Chen, M. Wang, X. Sheng, X. Chen, X. Feng, and S.S. Mao, *Prog. Mater Sci.* 98, 299 (2018).
13. F. Cao, J. Xiong, F. Wu, Q. Liu, Z. Shi, Y. Yu, X. Wang, and L. Li, *ACS Appl. Mater. Interfaces.* 8, 12239 (2016).
14. C. Stanley, A. Mojiri, and G. Rosengarten, *Nanophotonics* 5, 161 (2016).
15. C. Xiang, A.Z. Weber, S. Ardo, A. Berger, Y. Chen, R. Coridan, K.T. Fountaine, S. Haussener, S. Hu, R. Liu, N.S. Lewis, M.A. Modestino, M.M. Shaner, M.R. Singh, K. Sun, and K. Walczak, *Angew. Chem.* 55, 2 (2016).
16. V. Smirnov, K. Welter, F. Finger, F. Urbain, J.R. Morante, B. Kaiser, and W. Jaegermann, *Photoelectrochemical Solar Cell*, ed. N.D. Sankir and M. Sankir (Beverly: Scrivener Publishing, 2019), p. 351.
17. Harry L. Tuller, *Mater. Renew. Sustain Energy* 6, 3 (2017).
18. J. Jia, L.C. Seitz, J.D. Benck, Y. Huo, Y. Chen, J. Wei Desmond, T. Bilir, J.S. Harris, and T.F. Jaramillo, *Nat. Commun.* 7, 13237 (2016). https://doi.org/10.1038/ncomms13237.
19. E. Verlage, S. Hu, R. Liu, R.J.R. Jones, K. Sun, C. Xiang, N.S. Lewis, and H.A. Atwater, *Energy Environ. Sci.* 8, 3166 (2015).
20. R. van de Krol and M. Grätzel, *Photoelectrochemical Hydrogen Production* (New York: Springer, 2012).
21. K. Zakrzewska, K. Kollbek, M. Sikora, C. Kapusta, J. Szlachetko, M. Sitarz, M. Ziąbka, and M. Radecka, *Int. J. Hydrogen Energy* 40, 815 (2015).
22. A. Trenczek-Zając, E. Pamuła, M. Radecka, K. Kowalski, A. Reszka, A. Brudnik, E. Kusior, and K. Zakrzewska, *J. Nanosci. Nanotechnol.* 12, 4703 (2012).
23. M. Radecka, K. Zakrzewska, M. Wierzbicka, A. Gorzkowska, and S. Komornicki, *Solid State Ionics* 157, 379 (2003).
24. R.G. Breckenridge and W.R. Hosler, *Phys. Rev.* 91, 793 (1953).
25. R. Dannenberg and P. Green, *Thin Solid Films* 360, 122 (2000).
26. D. Mardare and G.I. Rusu, *Mater. Sci. Eng., B* 75, 68 (2000).
27. V. Lionas, T. Georgakopoulos, N. Todorova, S. Karapati, K. Pomoni, and C. Trapalis, *Mater. Sci. Semicond. Process.* 83, 63 (2018).
28. A. Yildiz, S.B. Lisesivdin, M. Kasap, and D. Mardare, *J. Non-Cryst. Solids* 354, 4944 (2008).
29. M. Kneiss, M. Jenderka, K. Brachwitz, M. Lorenz, and M. Grundmann, *Appl. Phys. Lett.* 105, 062103 (2014).
30. K. Pomoni, M.V. Sofianou, T. Georgakopoulos, N. Boukos, and C. Trapalis, *J. Alloys Compd.* 548, 294 (2013).
31. A. Yildiz, N. Serin, M. Kasap, T. Serin, and D. Mardare, *J. Alloys Compd.* 493, 227 (2010).
32. G. Gu, Z. He, Y. Tao, Y. Li, J. Li, H. Yin, W. Li, and Y. Zhao, *Vacuum* 70, 17 (2003).
33. D. Dorow-Gerspach and M. Wuttig, *Thin Solid Films* 669, 1 (2019).
34. M. Radecka, K. Zakrzewska, H. Czternastek, T. Stapiński, and S. Debrus, *Appl. Surf. Sci.* 65, 227 (1993).
35. B.-S. Jeong, D.P. Norton, and J.D. Budai, *Solid-State Electron.* 47, 2275–2278 (2003).
36. A. Trenczek-Zając, M. Radecka, K. Zakrzewska, A. Brudnik, E. Kusior, S. Bourgeois, M. Marco de Lucas, and L. Imhoff, *J. Power Sources* 194, 93 (2009).
37. K. Krówka, A. Wiatrowski, and W.M. Posadowski, *Thin Solid Films* 520, 4127 (2012).
38. K. Zakrzewska, A. Brudnik, M. Radecka, and W. Posadowski, *Thin Solid Films* 343–344, 152 (1999).
39. K. Zakrzewska, *Adv. Mater. Sci. Eng.* (2012). https://doi.org/10.1155/2012/826873.

40. A. Brudnik, H. Czternastek, K. Zakrzewska, and M. Jachimowski, *Thin Solid Films* 199, 45 (1991).
41. K. Zakrzewska, Titanium Dioxide Thin Films for Gas Sensors and Photonic Applications, AGH Uczelniane Wydawnictwa Naukowo-Dydaktyczne, Kraków 2003, Rozprawy Monografie 115, ISSN 0867-6631.
42. H. Koseoglu, F. Turkoglu, M. Kurt, M.D. Yaman, F.G. Akca, G. Aygun, and L. Ozyuzer, *Vacuum* 120, 8 (2015).
43. M. Losurdo, M. Giangregorio, P. Capezzuto, G. Bruno, R. De Rosa, F. Roca, C. Summonte, J. Pla, and R. Rizzoli, *J. Vac. Sci. Technol., A* 20, 37 (2002).

44. H. Kim, C.M. Gilmore, A. Piqué, J.S. Horwitz, H. Mattoussi, H. Murata, Z.H. Kafafi, and D.B. Chrisey, *J. Appl. Phys.* 86, 6451 (1999).
45. P. Drude, *Ann. Phys.* 306, 566 (1900).
46. T. Ohsaka, F. Izumi, and Y. Fujiki, *J. Raman Spectrosc.* 7, 321 (1978).